Journal of Power Sources 194 (2009) 1194–1201

Contents lists available at ScienceDirect

Journal of Power Sources

journal homepage: www.elsevier.com/locate/jpowsour

Facile approach to prepare loose-packed cobalt hydroxide nano-flakes materials for electrochemical capacitors

Ling-Bin Kong[a,b,*], Jun-Wei Lang[a], Min Liu[a], Yong-Chun Luo[b], Long Kang[b]

[a] State Key Laboratory of Gansu Advanced Non-ferrous Metal Materials, Lanzhou University of Technology, Lanzhou 730050, PR China
[b] Key Laboratory of Non-ferrous Metal Alloys and Processing of Ministry of Education, Lanzhou University of Technology, Lanzhou 730050, PR China

ARTICLE INFO

Article history:
Received 13 February 2009
Received in revised form 20 May 2009
Accepted 7 June 2009
Available online 16 June 2009

Keywords:
Electrochemical capacitors
Cobalt hydroxide
Specific capacitance
Nano-flakes
Pseudo-capacitance

ABSTRACT

Cobalt hydroxide nano-flakes are successfully synthesized by a facile chemical precipitation method. Electrochemical characterization is performed using cyclic voltammetry, chronopotentiometry and impedance spectroscopy, respectively. These cobalt hydroxide nano-flakes maintain high utilization at high rates of discharge. A maximum specific capacitance of 735 F g^{-1} can be achieved in 2 M aqueous KOH with the potential range from −0.2 to 0.4 V (vs. SCE) in a half-cell setup configuration for the nano-flakes $Co(OH)_2$ electrode, suggesting its potential application in electrochemical capacitors. Furthermore, the effect of annealing temperatures on the electrochemical capacitance characteristics is also been systematically explored.

1. Introduction

Research into nanomaterials has increased recently due to their unique electrical, optical, magnetic, and catalytic characteristics in comparison with the bulk materials. Numerous research groups in both academia and industry around the world are consciously increasing efforts towards designing and developing advanced materials with dimensions ranging from a few to several hundred nanometers [1,2]. Recently, nanostructured electrode materials have attracted great interest, as the capability of electrode materials for electrochemical capacitor system is significantly influenced by its surface area and morphology, thereby, the synthesis of nanostructured, high surface area and high porous materials is an important point because the high surface area produces the large reaction place and a lot of pores cause rapid transfer of the electrolyte [3,4].

Electrochemical capacitors, also called supercapacitors, combining the advantages of dielectric capacitors, which can deliver high power within a very short time, and rechargeable batteries, which can store high amounts of energy, have found an increasingly important role in power-source applications such as hybrid electric vehicles, short-term power sources for mobile electronic devices, etc. [5–7]. Therefore, a lot of research work has been done in the past few years to improve the performance of the electrochemical capacitor electrode.

The electrochemical capacitors are generally classified into two types: (i) most notably double-layer capacitance arising from the charge separation at the electrode/electrolyte interface and (ii) faradaic pseudo-capacitance arising from fast, reversible electrosorption or redox processes occurring at or near the solid electrode surface [8]. The large specific capacitance of electrochemical capacitors is the result of one or a combination of these charge-storage mechanisms. Moreover, the energy density of the relatively new pseudocapacitor devices that are based on faradaic processes has been reported many times, because it has been recognized that the energy density based on pseudo-faradaic processes is of many times greater than that of the traditional double-layer capacitors (its capacitance is typically less than 20 μF cm^{-2}) [9,10].

The power density of electrochemical capacitors is the most attractive property. However, the lower energy density of electrochemical capacitors compared to that of secondary battery is a drawback for practical devices such as electric vehicles [11]. From a materials point of view, there are three main categories of electrochemical capacitors: carbon [11,12], metal oxide [1,13], and electronically conducting polymer [14,15]. Among these electrode materials, the capacitances of metal oxide and conducting-polymer electrode mainly results from the pseudo-capacitance which originate from the electrical charge transport in redox reaction. Conducting-polymer capacitors have been reported to display high power densities, but their specific capacitances are much lower

* Corresponding author at: State Key Laboratory of Gansu Advanced Non-ferrous Metal Materials, Lanzhou University of Technology, 287 Langongping Road, Lanzhou 730050, PR China. Tel.: +86 931 2976579; fax: +86 931 2976578.
E-mail address: konglb@lut.cn (L.-B. Kong).

0378-7753/$ – see front matter © 2009 Elsevier B.V. All rights reserved.
doi:10.1016/j.jpowsour.2009.06.016

than that of metal-oxide capacitors. It is well known that hydrated ruthenium oxide is an excellent material with remarkable high specific capacitance values ranging from 720 to 760 F g^{-1} (for single electrode system) [16,17]. However, the high cost of raw materials has prevented this material from commercial applications. Hence, much effort has been made to search for alternative inexpensive electrode materials with good capacitive characteristics, such as CoO_x [18,19], NiO [20,21], MnO_2 [22,23], $Co(OH)_2$ [4], $Ni(OH)_2$ [24], etc. Among the transitional base metal oxides, cobalt compounds capacitors are studied as cheaper candidates with good capacitive characteristics due to its many important technological applications.

There are several methods used to prepare cobalt oxides such as chemical precipitation [25], electrodeposition [26], and sol–gel technique [7]. However, these processes largely lead to micrometer cobalt oxides or aggregated nanostructural cobalt oxides with a low specific capacitance. Therefore, a lot of research work has been done to improve the electrochemical performance of cobalt oxides. The cobalt hydroxides are known to crystallize in two polymorphic modifications known as α and β. The distinguishing feature of α-$Co(OH)_2$ is its larger interlayer spacing compared to that of the β-form, on account of which the α-form has a higher electrochemical activity and an interesting interlayer chemistry. There is therefore considerable interest in synthesizing the α-$Co(OH)_2$ material for electrochemical capacitors [27]. In this work, we report a facile chemical precipitation method to prepare the cobalt hydroxide materials. The studies show that the as-prepared $Co(OH)_2$ material was corresponds to the layered α-$Co(OH)_2$ with low crystallinity and nano-flake network structure. The effect of reaction time on the microstructure and morphology of the $Co(OH)_2$ samples was also observed systematically, at the same time, the forming mechanism of nano-flake structured $Co(OH)_2$ is presented and discussed. The as-prepared $Co(OH)_2$ material possesses a narrow mesoporous distribution at around 5–20 nm and has a surface area of about 85.4 m^2 g^{-1}. We demonstrate that the unique microstructure creates electrochemical accessibility of electrolyte OH^- ions to $Co(OH)_2$ nano-flakes and a fast diffusion rate within the redox phase. Electrochemical measurements were carried out in 2 M aqueous KOH in a half-cell setup configuration at room temperature using cyclic voltammetry (CV), chronopotentiometry and impedance spectroscopy, respectively. The maximum specific capacitance of 735 F g^{-1} is the highest report of pure $Co(OH)_2$ for electrochemical capacitors, which shows better rate capability and great potential as the electrode materials for electrochemical capacitors. In addition, the effect of annealing temperatures on the capacitance property of $Co(OH)_2$ was also studied in detail.

2. Experimental

2.1. Preparation of the $Co(OH)_2$ powder

All of the chemicals were of analytical grade and used without further purification. $Co(OH)_2$ materials were prepared by a facile improved precipitation method. The first step was the confecting of cobalt chloride hydrate solution (1 M, 25 ml) in a glass beaker, using a magnetic stir bar. The cobalt chloride hydrate solution was slowly adjusted to pH 9 by dropwise addition of 5 wt.% $NH_3{\cdot}H_2O$ (30 ml) at a temperature of ~10 °C, the $NH_3{\cdot}H_2O$ was added dropwise with a constant time interval of 5 s. The resulting suspension was stirred at this temperature for an additional 3 h. Then the solid was filtered, washed with a copious amount of distilled water several times. The obtained product was dried at different temperature in air at 100, 150, 200, 250, 300, 350 °C, respectively, for 6 h (without special denotation, the $Co(OH)_2$ sample is referred to annealing at 100 °C in this work).

2.2. Preparation of the electrode

The working electrodes were prepared according to the method reported in literature [22]. 80 wt.% of $Co(OH)_2$ powder was mixed with 7.5 wt.% of acetylene black (>99.9%) and 7.5 wt.% of conducting graphite in an agate mortar until a homogeneous black powder was obtained. To this mixture, 5 wt.% of poly (tetrafluoroethylene) was added with a few drops of ethanol. After briefly allowing the solvent to evaporate, the resulting paste was pressed at 10 MPa to a nickel gauze with a nickel wire for an electric connection. The electrode assembly was dried for 16 h at 80 °C in air. Each electrode contained about 8 mg of electroactive material and had a geometric surface area of about 1 cm^2.

2.3. Structure characterization

The obtained products were characterized by transmission electron microscope (JEOL, JEM-2010, Japan), field emission scanning electron microscope (JEOL, JSM-6701F, Japan), X-ray diffraction measurements (Rigaku, D/Max-2400, Japan), Thermogravimetric analysis (Netzsch, STA-449C, Germany) and nitrogen adsorption and desorption experiments (Micromeritics, ASAP 2010M, USA). The surface area was calculated using the Brunauer–Emmett–Teller (BET) equation. Pore-size distributions were calculated by the Barrett–Joyner–Halenda (BJH) method using the desorption branch of the isotherm.

2.4. Electrochemical measurements

Electrochemical measurements were carried out using an electrochemical working station (CHI660C, Shanghai, China) in a half-cell setup configuration at room temperature. A platinum gauze electrode and a saturated calomel electrode served as the counter electrode and the reference electrode, respectively. CV scans were recorded from −0.3 to 0.5 V (vs. SCE) at different scan rate in 2 M KOH aqueous solution, and charge–discharge cycle tests were carried out in the potential range of −0.2 to 0.4 V in 2 M KOH aqueous solution at different constant current densities. Electrochemical impedance spectroscopy measurements were performed under open circuit potential in an a.c. frequency range from 10,000 to 0.01 Hz with an excitation signal of 5 mV. All electrochemical experiments were carried out at 20 ± 1 °C.

3. Results and discussion

3.1. Characterization of materials

TGA was conducted for as-prepared $Co(OH)_2$ materials in argon atmosphere to examine the conversion process during calcinations. Shown in Fig. 1, the sample weight decreases slowly between 100 and 150 °C, this is expected to be due mainly to the removal of chemically adsorbed H_2O; a obvious weight loss of 10.39% is present between 150 and 300 °C on the TG curve, it is believed that the thermal decomposition take places leading to the formation of Co_3O_4 in this region; when the temperature is above 300 °C, the TG curve becomes flat, which indicates that no phase transformation occurs, and further heating could only make the structure of the products more crystalline, which is confirmed by the following XRD results.

Shown in Fig. 2 are the XRD patterns of the $Co(OH)_2$ material and the corresponding samples heated at different temperatures for 6 h in air. No obvious peaks of β-$Co(OH)_2$ have been observed in the XRD pattern of the as-prepared $Co(OH)_2$ material obtained at 100 °C, and it correspond to the layered α-$Co(OH)_2$ structure (PDF, card no. 46-0605) with low crystallinity [27]. Being heated at 150 °C for 6 h, almost all peaks can be indexed to the diffraction data of the spinel structure Co_3O_4 (PDF, card no. 42-1467). Along

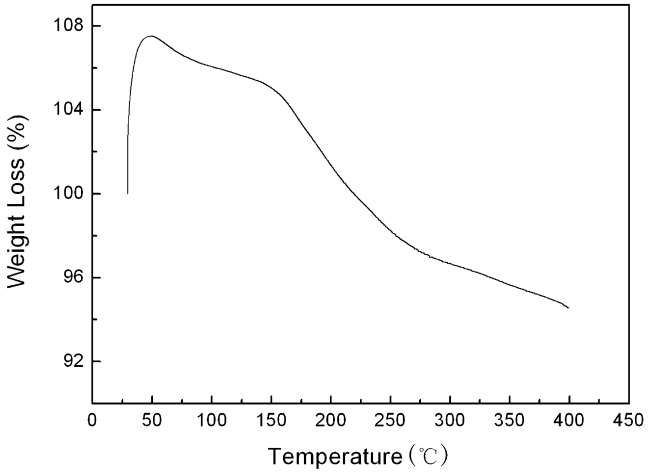

Fig. 1. TG plots of as-prepared $Co(OH)_2$ material.

with the increase of the anneal temperature, X-ray diffraction peaks of as-prepared samples gradually strengthen and narrow. The considerable broadening of diffraction peaks (especially for $Co(OH)_2$ sample) demonstrates the presence of particles made of very small $Co(OH)_2$ crystals [28]. This result is in agreement with that of the TG analysis.

SEM and TEM measurement were performed to the as-prepared $Co(OH)_2$ materials. The morphologies of $Co(OH)_2$ can be seen in Fig. 3a and c. It is noteworthy that the network-like structure (which consists of interconnected nano-flakes) shows anisotropic morphology characteristics and the formation of a loosely packed microstructure in the nanometer scale. The unique structure plays a basic role in the morphology requirement for electrochemical accessibility of electrolyte OH^- to $Co(OH)_2$ active material and a fast diffusion rate within the redox phase. It is believed that the unique structure provided an important morphological foundation for the extraordinary high specific capacitances. When $Co(OH)_2$ was transformed to Co_3O_4 at the subsequent annealing process, most of the nano-flakes grow to a stacking structure because H_2O will be lost as the annealing temperature increases. Just shown in Fig. 3b and d, the particles and nano-flakes phase both appeared in the Co_3O_4 samples.

Fig. 4 illustrates the schematic formation mechanism of cobalt hydroxide aggregates. As $NH_3{\cdot}H_2O$ solution was added into the cobalt chloride solution dropwise, numerous nucleation centers can be formed in the solution. That result in more and more $Co(OH)_2$ deposited extending around the nucleation to form the amorphous particles. When pH is increased by $NH_3{\cdot}H_2O$ titration, the growing point of each crystal is located at certain directions, so nano-flakes will grow up around the nucleation centers at the surface of the particle because of the anisotropy of $Co(OH)_2$ crystals. As a result, the microsphere of nano-flakes will be formed. With the reaction going on, new $Co(OH)_2$ nano-flakes will grow up around the nucleation centers at the surface of the microsphere. The surface growth leads to continuous increase in size and density of the microsphere to form a network structure.

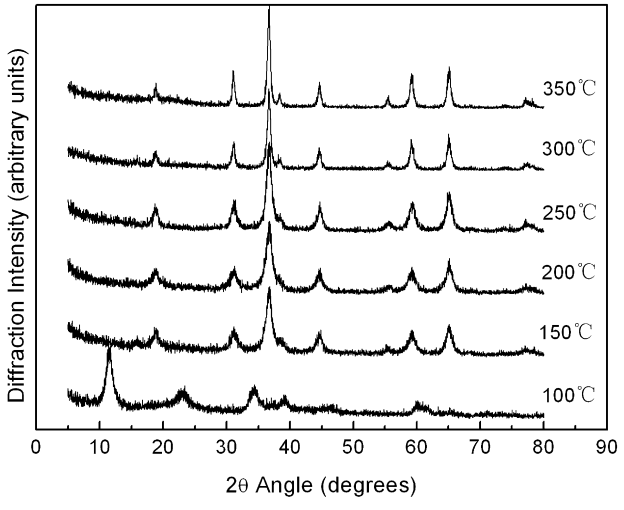

Fig. 2. The XRD patterns of the $Co(OH)_2$ material and the corresponding samples heated at different temperatures for 6 h in air.

In order to confirm the crystal growth mechanism of the $Co(OH)_2$ nano-flakes, we synthesized $Co(OH)_2$ samples a, b, c and d corresponding to the different volume of $NH_3{\cdot}H_2O$ solution of 1.25, 2.5, 5 and 30 ml, respectively. The $NH_3{\cdot}H_2O$ was added dropwise with a constant time interval of 5 s, and the resulting suspension was filtered, washed with a copious amount of distilled water without any aging. The effect of the reaction time on the microstructure and morphology of the samples was observed by field emission scanning electron microscope systematically. The high-magnification SEM images of the different samples are shown in Fig. 5. The morphology in Fig. 5a show that the original sample is amorphous particles; the tendency of nano-flakes growing at the surface of the particle can be found in Fig. 5b; it is noteworthy that the network-like structure, which consists of interconnected rough nano-flakes, can be seen in Fig. 5c; the network-like structure in Fig. 5d is uniform, just as the final product. This results confirmed the crystal growth mechanism of the $Co(OH)_2$ nano-flakes mentioned above.

It is generally known that the BET surface area and pore-size distributions are directly correlated to the specific capacitance. Surface area and pore-size distribution analysis of these materials were conducted using N_2 adsorption and desorption experiments. As seen from Fig. 6a and b, the profile of the hysteresis loop indicates an adsorption–desorption characteristics of the porous materials. The BET specific surface area of the $Co(OH)_2$ materials obtained at 100 and 250 °C were 85.4 and 71 $m^2\,g^{-1}$, respectively. Fig. 6c shows the pore diameter distributions of these two samples. As shown in this figure, the $Co(OH)_2$ materials obtained at 100 °C possess a narrow mesoporous distribution at around 4–20 nm. When the materials were subjected to a higher heat-treatment temperature, some of the $Co(OH)_2$ nano-flakes grew to a staking particles and the pore diameter increased, as a result, the specific surface decreased. The $Co(OH)_2$ materials obtained at 250 °C possess a broad mesoporous distribution at around 5–50 nm. Since the size range of the hydrated ions in the electrolyte is typically 6–7.6 Å, and the pore size at the range of 8–50 Å is the effective one required to increase either the pseudo-capacitance or electric double-layer capacitance [28]. The obtained high specific capacitance of 735 $F\,g^{-1}$ from the synthesized $Co(OH)_2$ materials obtained at 100 °C is mainly attributed to the effective distributions of the pore size and high specific surface area.

3.2. Electrochemical test

3.2.1. Cyclic voltammetry and discharge tests of the $Co(OH)_2$ electrode

CV and chronopotentiometry measurements have been used to evaluate the electrochemical properties and quantify the specific capacitance of the as-prepared $Co(OH)_2$ electrodes. Fig. 7a shows the CV curves of the $Co(OH)_2$ electrode at various sweep rates. The shapes of the CV reveal that the capacitance characteristic is well distinguished from that of the electric double-layer capacitance in which the shape is normally close to an ideal rectangular shape. According to the literature [18], two plausible reactions may occur

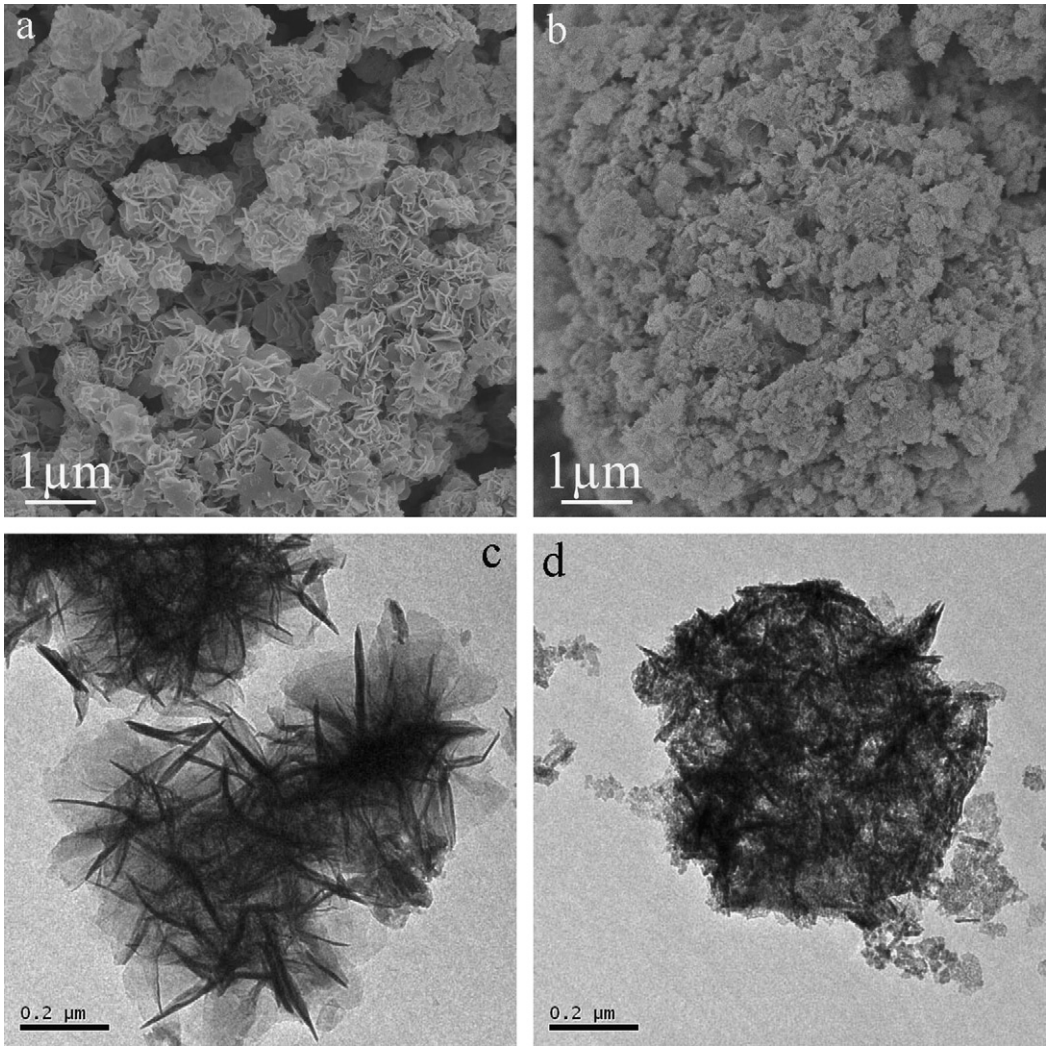

Fig. 3. SEM (a and b) and TEM (c and d) image of $Co(OH)_2$ and Co_3O_4 samples.

as quasi-reversible redox processes during the potential sweep of the $Co(OH)_2$ electrode:

$$Co(II)_s + OH^- \leftrightarrow Co(II)(OH)_{ad} + e^-$$
$$Co(II)(OH)_{ad} \leftrightarrow Co(III)(OH)_{ad} + e^- \quad (1)$$

$$Co(III)_s + OH^- \leftrightarrow Co(III)(OH)_{ad} + e^-$$
$$Co(III)(OH)_{ad} \leftrightarrow Co(IV)(OH)_{ad} + e^- \quad (2)$$

The anodic peak P1 is due to the oxidation of Co(II) to Co(III) and the cathodic peak P2 is for the reverse process. The anodic peak P3 is due to the oxidation of Co(III) to Co(IV) and the cathodic peak P4 is for the reverse process. It should be noted that with the increase of sweep rate, the shape of the CV changed, anodic peak potential and cathodic peak potential shift in the more anodic and more cathodic direction, and the capacitance, inevitably, decreased, which is in agreement with the result of chronopotentiometry measurement.

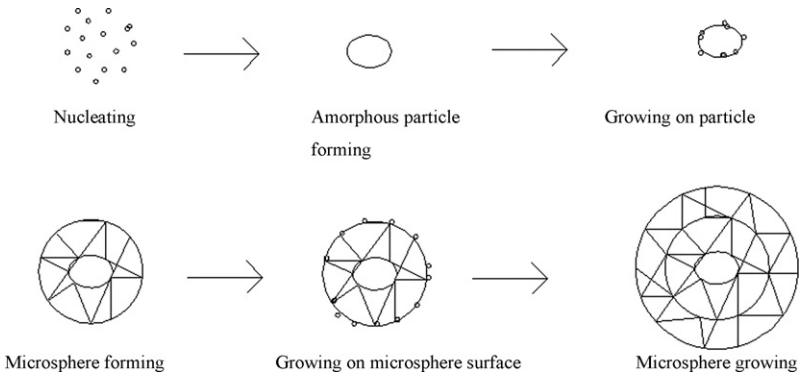

Fig. 4. Schematic formation mechanism of the as-prepared $Co(OH)_2$ material.

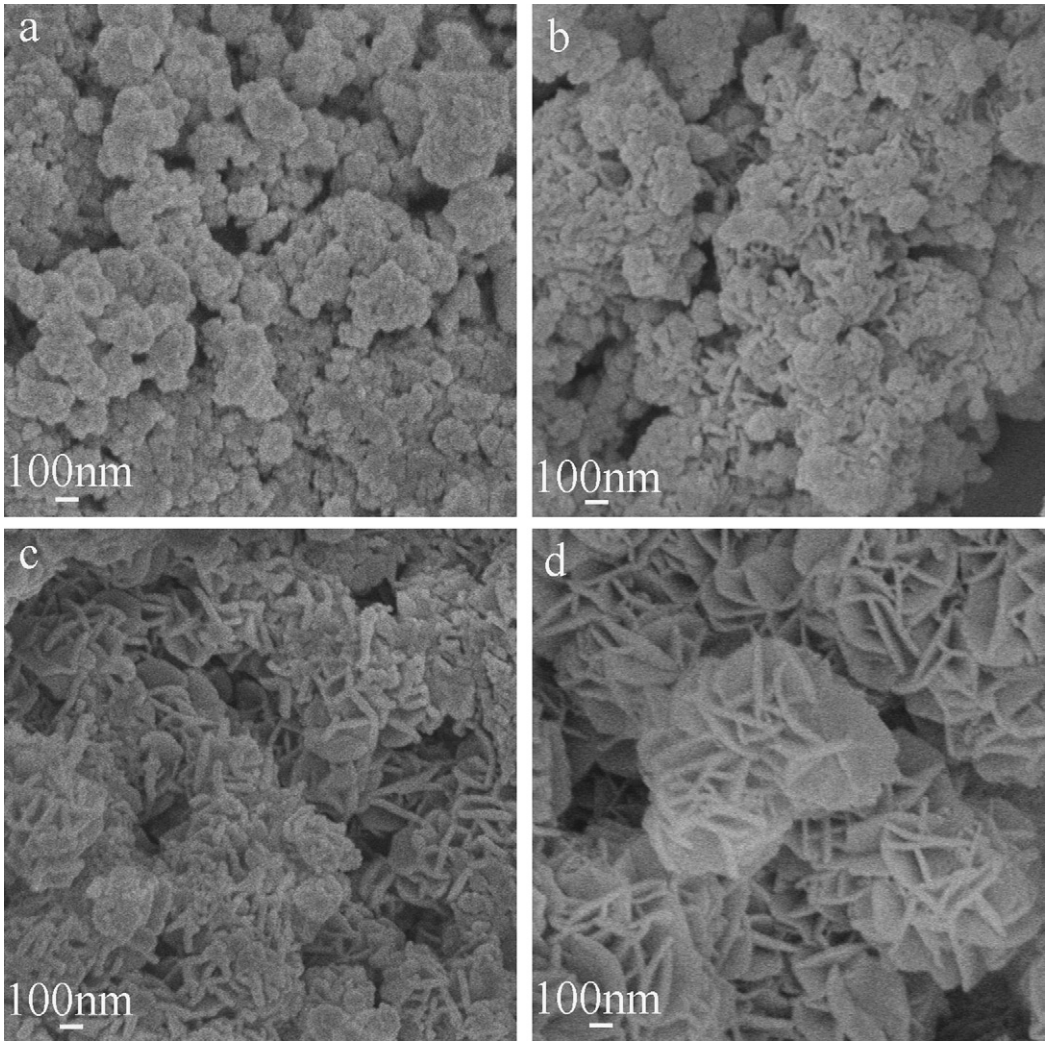

Fig. 5. The SEM images of the different $Co(OH)_2$ samples based on changing the volume of $NH_3{\cdot}H_2O$ solution: (a) 1.25 ml; (b) 2.5 ml; (c)5 ml and (d) 30 ml.

In practice, the ability to discharge at high rate is crucial in capacitors. The relationship between specific capacitance and current density is therefore investigated, and Fig. 7b shows the results. The specific capacitance of the $Co(OH)_2$ electrode is obtained in the potential range of −0.2 to 0.4 V in 2 M KOH at various current densities (5, 10, 20 and 30 mA cm^{-2}). The corresponding specific capacitance was calculated from $C = I/[(dE/dt) \times m] \approx I/[(\Delta E/\Delta t) \times m]$, where I is the constant discharging current, dE/dt indicates the slope of the discharge plot of the discharging curves, and m is the mass of the corresponding electrode materials measured. In this way, the specific capacitance of the $Co(OH)_2$ materials at 5, 10, 20 and 30 mA cm^{-2} were 735, 702, 637.5 and 609 F g^{-1}. This result indicates that the nano-flake structure increases the specific capacitance of $Co(OH)_2$ greatly. The shape of the discharge curves does not show the characteristic of pure double-layer capacitor, but mainly pseudo-capacitance, which are in agreement with the result of the CV curves. The curves obviously display two variation ranges, a linear variation of the time dependence of the potential (below about −0.05 V) indicates the double-layer capacitance behavior, which is caused by the charge separation taking place between the electrode and electrolyte interface, and a slope variation of the time dependence of the potential (from 0.4 to −0.05 V) indicates a typical pseudo-capacitance behavior, which resulted from the electrochemical adsorption/desorption or redox reaction at an interface between electrode and electrolyte [29]. Fig. 7b also shows that the $Co(OH)_2$ electrode prepared exhibits good rate capability. As discharge current increases, the large voltage drop is produced, and finally the capacitance decreases. This phenomenon may be explained by referring to OH^- ions diffusion processes during the charging/discharging for the electrode. When the electrode at high sweep rates corresponding to high current density massive OH^- ions are required to intercalate swiftly at the interface of electrode/electrolyte, however, relatively low concentration of OH^- ions could not meet this demand and the processes would be controlled by the ion diffusion [30]. However, the discharge capacitance at 10 mA is 95.5% of that discharged at 5 mA cm^{-2}, so the excellent rate capability of the sample makes it attractive particularly for a practical application. This all demonstrate that the unique microstructure creates electrochemical accessibility of electrolyte OH^- ions to $Co(OH)_2$ nano-flakes and a fast diffusion rate within the redox phase.

3.2.2. Effects of annealing temperature on specific capacitance of cobalt hydroxide

To evaluate the electrochemical capacitance of the $Co(OH)_2$ samples as a function of the heating temperatures, the chronopotentiometry measurements were conducted to $Co(OH)_2$ samples with different annealing temperatures. Fig. 8a shows the discharging curves at the discharging current of 5 mA of the $Co(OH)_2$

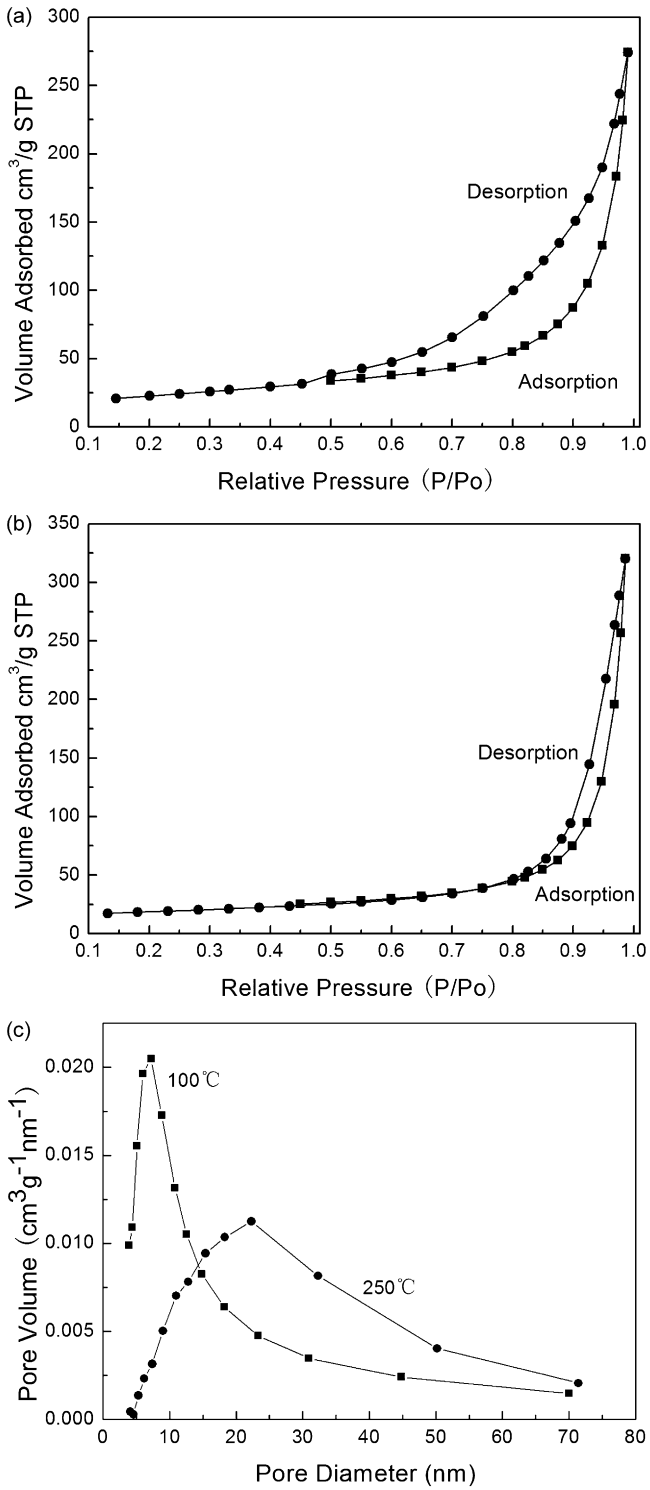

Fig. 6. (a) The N_2 adsorption–desorption isotherm of $Co(OH)_2$ materials obtained at 100 °C and (b) 250 °C; (c) The BJH pore-size distributions of $Co(OH)_2$ materials obtained at 100 and 250 °C.

materials and corresponding samples heated at different temperatures. With increasing annealing temperature, $Co(OH)_2$ material converted to Co_3O_4, and the increased pore diameter can enhance the diffusivity of the electrolyte ions in the pores, and this resulted in the increase of the discharging plateau. Fig. 8b shows the effect of annealing temperature on the capacitive properties of the $Co(OH)_2$ electrodes. With increasing annealing temperature, and decline tendency of the specific capacitance is similar and relevant to different discharge currents. The decrease in the capacitance characteristic was mainly attributed to the decreased specific surface area resulting from the disrepair of the nano-flakes and the increased particle diameter. With increasing annealing temperature, the physical and chemical water removed, once the oxide phase is formed, further heat-treatment at higher temperature may cause the increase in pore diameter, and accordingly the decrease in specific surface area and, also possibly, its reactivity for surface chemical process, thereby leading to a decreased capacitance [20]. Fig. 8b also shows that all the $Co(OH)_2$ samples exhibit good rate capability.

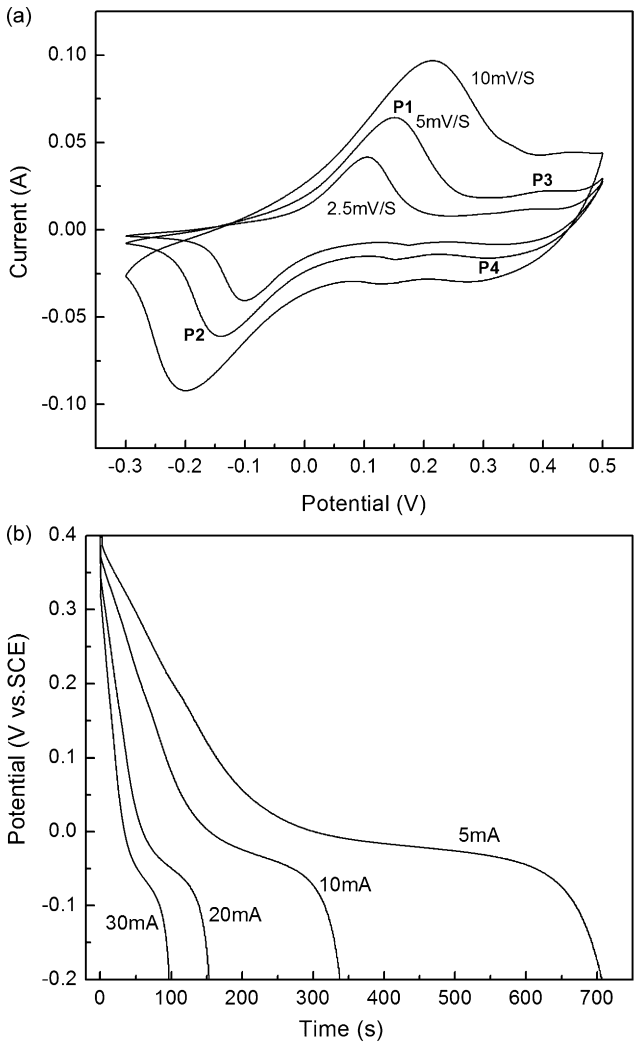

Fig. 7. Electrochemical properties of $Co(OH)_2$ electrode in 2 M KOH solution: (a) CV curves at different scan rates; (b) discharging curves at different discharging currents.

3.2.3. *Electrochemical impedance spectroscopy tests*

The electrochemical impedance measurements were carried out on the $Co(OH)_2$ electrodes at 0.392 V (vs. SCE). The typical results are shown in Fig. 9. The complex-plane impedance plots for each sample can be divided into the high-frequency component and the low-frequency component. A distinct knee in the frequency can be observed in curves of Fig. 9. From the point intersecting with the real axis in the range of high frequency, the internal resistances (which is equal to R_b) of the $Co(OH)_2$ electrodes are 1.25, 1.2, 1.17, 1.14, 1.13 and 1.1 Ω, corresponding to the $Co(OH)_2$ samples obtained at 100, 150, 200, 250, 300 and 350 °C, respectively. It includes the total resistances of the ionic resistance of electrolyte, intrin-

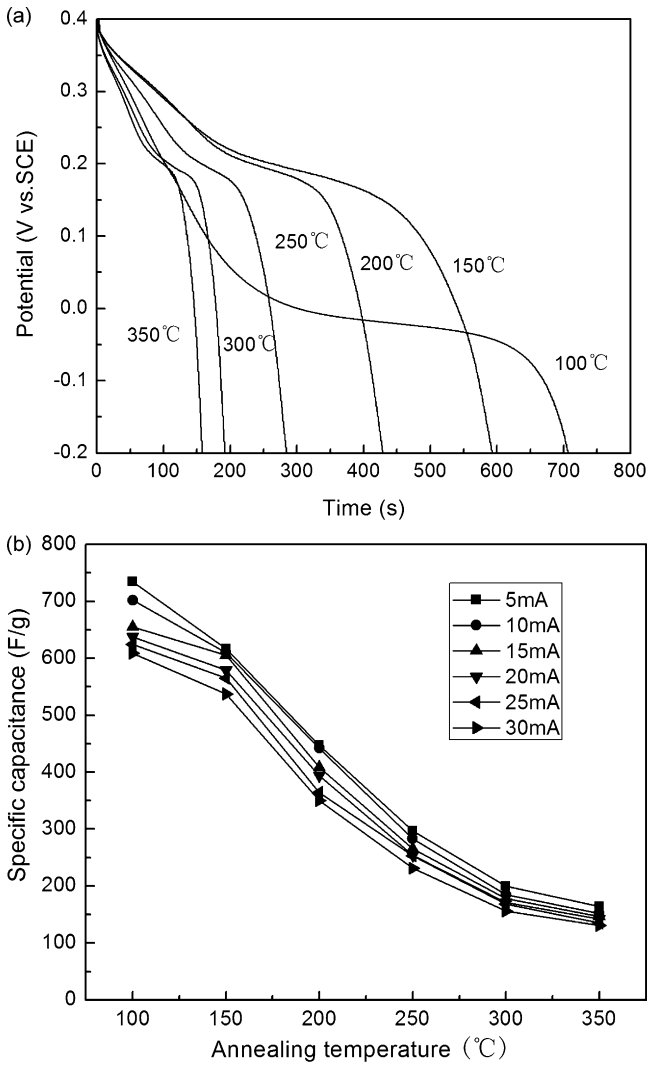

Fig. 8. Electrochemical properties of $Co(OH)_2$ materials and corresponding samples heated at different temperatures in 2 M KOH solution: (a) discharging curves in the potential range from 0.4 to −0.2 V at the discharging current of 5 mA; (b) the specific capacitance as a function of discharge currents.

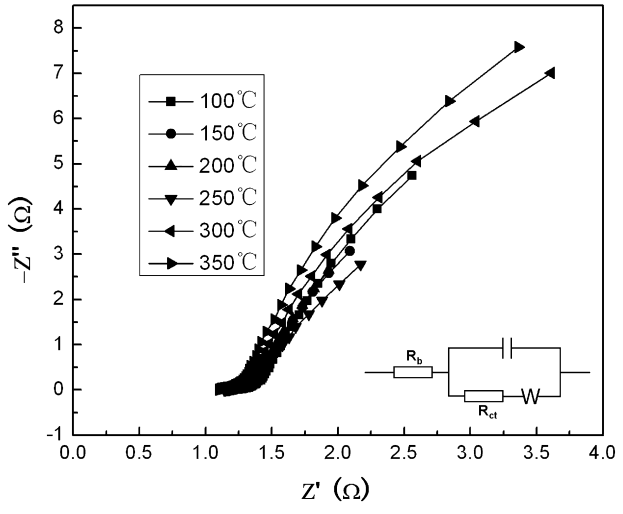

Fig. 9. Complex-plane impedance plots of the $Co(OH)_2$ electrode prepared at different heat-treatment temperatures (0.392 V vs. SCE; electrolyte: 2 M KOH). The inset is the equivalent circuit.

sic resistance of active materials and contact resistance at the active material/current collector interface. This can be explained that with the increase in the heat-treatment temperature, the increase in the pore diameter can enhance the diffusivity of the electrolyte ions in the pores. However, the overall decreasing equivalent series resistance conductive to increase capacitance cannot compensate for the loss of the capacitance due to the decreased specific surface area resulting from the disrepair of the nano-flakes and the increased particle diameter. The semicircle in the high-frequency range associates with the surface properties of porous electrode corresponds to the faradic charge-transfer resistance (R_{ct}). It can be seen that all the $Co(OH)_2$ and Co_3O_4 samples have small charge-transfer resistance. At the lower frequencies, a straight sloping line represents the diffusive resistance (Warburg impendence) of the electrolyte in electrode pores and the proton diffusion in host materials. The phase angles for impedance plots of all the $Co(OH)_2$ and Co_3O_4 electrodes were observed to be higher than 45° in the low frequencies clearly. These findings suggest that all the electrodes are not strongly controlled by diffusion process, implying the good accessibility of the ions and/or the possible contributions of electrochemical capacitors [31,32].

4. Conclusions

In summary, we have synthesized loose-packed α-$Co(OH)_2$ materials consisting of nano-flake network using a facile chemical precipitation method, and applied its microstructure for electrochemical capacitors. The XRD, SEM, TEM and BET specific surface area studies show that the as-prepared $Co(OH)_2$ materials have a less crystallization, nano-flake structure, a high specific surface area of 85.4 $m^2\,g^{-1}$ and a narrow mesoporous distribution at around 4–20 nm. The unique microstructure can accommodate the electroactive species in the solid bulk electrode material. The specific capacitance of the $Co(OH)_2$ electrode at 5, 10, 20 and 30 mA cm^{-2} were 735, 702, 637.5 and 609 F g^{-1}, which shows better rate capability and great potential as the electrode materials for electrochemical capacitors. The maximum specific capacitance is the highest report for $Co(OH)_2$ electrode. Even though we do not fully understand the fundamental structure of $Co(OH)_2$ materials, the strategy reported here should be viable to extend to other transition metal-oxide systems.

Acknowledgements

This work is supported by the National Natural Science Foundation of China (No. 50602020), the Natural Science Foundation of Gansu Province (No. 0803RJZA002) and the Program for Outstanding Young Teachers in Lanzhou University of Technology (No. Q200803).

References

[1] L. Cao, F. Xu, Y.Y. Liang, H.L. Li, Adv. Mater. 16 (2004) 1853–1857.
[2] M. Mo, J.C. Yu, L.Z. Zhang, S.K.A. Li, Adv. Mater. 17 (2005) 756–760.
[3] H. Zhou, D. Li, M. Hibino, I. Honma, Angew. Chem. Int. Ed. 14 (2005) 797–802.
[4] E. Hosono, S. Fujihara, I. Honma, M. Ichihara, H. Zhou, J. Power Sources 158 (2006) 779–783.
[5] B.E. Conway, Electrochemical Supercapacitors Scientific Fundamentals and Technological Applications, Kluwer Academic/Plenum Publishers, New York, 1999.
[6] M. Winter, R.J. Brodd, Chem. Rev. 104 (2004) 4245–4269.
[7] C. Lin, J.A. Ritter, B.N. Popov, J. Electrochem. Soc. 145 (1998) 4097–4103.
[8] S.C. Pang, M.A. Anderson, T.W. Chapman, J. Electrochem. Soc. 147 (2000) 444–450.
[9] K.R. Prasad, K. Koga, N. Miura, Chem. Mater. 16 (2004) 1845–1847.
[10] B.V. Tilak, C.P. Chen, J. Electrochem. Soc. 143 (1996) 3791–3799.
[11] K.H. An, W.S. Kim, Adv. Funct. Mater. 11 (2001) 387–392.
[12] D.W. Wang, F. Li, M. Liu, G.Q. Lu, H.M. Cheng, Angew. Chem. Int. Ed. 47 (2008) 373–376.
[13] Y.F. Ke, D.S. Tsai, Y.S. Huang, J. Mater. Chem. 15 (2005) 2122–2127.

[14] L.Z. Fan, Y.S. Hu, J. Maier, P. Adelhelm, B. Smarsly, M. Antonietti, Adv. Funct. Mater. 17 (2007) 3083–3087.
[15] W.C. Chen, T.C. Wen, H. Teng, Electrochim. Acta 48 (2003) 641–649.
[16] J.P. Zheng, P.J. Cygan, T.R. Jow, J. Electrochem. Soc. 142 (1995) 2699–2703.
[17] T. Cottineau, M. Toupin, T. Delahaye, T. Brousse, D. Bélanger, Appl. Phys. A 82 (2006) 599–606.
[18] S. Palmas, F. Ferrara, A. Vacca, M. Mascia, A.M. Polcaro, Electrochim. Acta 53 (2007) 400–406.
[19] V.R. Shinde, S.B. Mahadik, C.D. Gujar, C.D. Lokhande, Appl. Surf. Sci. 252 (2007) 7487–7492.
[20] V. Srinivasan, J.W. Weidner, J. Electrochem. Soc. 144 (1997) L210–L213.
[21] M.Q. Wu, J.H. Gao, S.R. Zhang, A. Chen, J. Porous Mater. 13 (2006) 407–412.
[22] M. Toupin, T. Brousse, D. Bélanger, Chem. Mater. 16 (2004) 3184–3190.
[23] C.C. Hu, T.W. Tsou, Electrochim. Acta 47 (2002) 3523–3528.
[24] L. Cao, L.B. Kong, Y.Y. Liang, H.L. Li, Chem. Commun. 14 (2004) 1646–1647.
[25] Y.Y. Liang, L. Cao, L.B. Kong, H.L. Li, J. Power Sources 136 (2004) 197–200.
[26] V. Srinivasan, J.W. Weidner, J. Power Sources 108 (2002) 15–20.
[27] M. Rajamathi, P.V. Kamath, R. Seshadri, Mater. Res. Bull. 35 (2000) 271–278.
[28] L. Cao, M. Lu, H.L. Li, J. Electrochem. Soc. 152 (2005) A871–A875.
[29] D.D. Zhao, S.J. Bao, W.J. Zhou, H.L. Li, Electrochem. Commun. 9 (2007) 869–874.
[30] R. Kötz, M. Carlen, Electrochim. Acta 45 (2000) 2483–2498.
[31] M.W. Xu, D.D. Zhao, S.J. Bao, H.L. Li, J. Solid State Electrochem. 11 (2007) 1101–1107.
[32] S.S. Zhang, K. Xu, T.R. Jow, Electrochim. Acta 49 (2004) 1057–1061.